



## Petrogenesis of the Neoproterozoic rocks of Megele area, Asosa, Western Ethiopia

Temesgen Oljira<sup>1,4\*</sup>, Olugbenga Akindeji Okunlola<sup>2</sup>, Akinade Shadrach Olatunji<sup>2</sup>, Dereje Ayalew<sup>3</sup>, Bekele Ayele Bedada<sup>1</sup>

1. Department of Geology, Pan African University, Life and Earth Sciences Institute, University of Ibadan, Ibadan, Nigeria. as.olatunji@mail.ui.edu.ng, bekele@hu.edu.et

2. Department of Geology, University of Ibadan, Ibadan, Nigeria. o.okunlola@mail.ui.edu.ng

3. School of Earth Sciences, Addis Ababa University, P. O. Box 1176, Addis Ababa, Ethiopia.

4. Department of Geology, Adama Science and Technology University, Adama, Ethiopia.

### ABSTRACT

The Western Ethiopian Shield is underlain by volcano-sedimentary terranes, gneissic terranes, and ophiolitic rocks intruded by different granitoid bodies. The Megele area is part of Western Ethiopian Shield and consist of a low-grade volcano-sedimentary zone that has been intruded by mafic (dolerite dyke) and granitoid intrusions (granodiorite, diorite, granite gneiss). To establish the origin of the distinctive lithologies of the locality and evaluate its mineral potential, petrological, petrographical, and geochemical characterization of these rocks were carried out. Hence, the lithological, geochemical, and petrogenetic features of the Neoproterozoic granitoid intrusives and associated metavolcanic, were illustrated through a combination of field mapping, petrological, and geochemical analysis. The petrological result obtained from the thin section analysis of the granitoids and metabasalt from Megele area indicates that, these rocks has been metamorphosed from lower green-schist facies to lower amphibolite facies as denoted by mineral assemblages such as albite + muscovite + prehnite+ quartz and actinolite + hornblende + epidote + garnet. The major and trace element geochemical analysis of granodiorite, diorite, and granite gneiss revealed that the rocks in the studied area were mainly calc-alkaline and peraluminous in nature in the  $\text{SiO}_2$  versus  $\text{Na}_2\text{O}+\text{K}_2\text{O}$  and A/NK versus A/CNK, the details of the results on the major and rare elements are stated in the result section respectively. The granitoids are S-type granites revealed silica saturated rock formed at the volcanic arc subduction (VAG) to syn-collisional (syn-COLD) tectonic setting by fractionation of LREE-enriched, HREE-depleted basaltic magma with considerable crustal input. This basaltic magma seems to be generated from the LREE-enriched, HREE-depleted mantle. In conclusion, the metabasalt is sub-alkaline (tholeiitic), metaluminous bodies generated at mid-oceanic ridge tectonic setting by partially melting of HREE-depleted and LREE-enriched basaltic magma. The magma sources are associated with the reworked sediment-laden crustal slabs from the subduction zone and resulted in S-type granitoid.

**Keywords:** Fractional crystallization; Geochemistry; Megele; Neoproterozoic; Petrogenesis; S-type granite.

## Petrogénesis de rocas Neoproterozoicas del área de Megele, Oeste de Etiopía

### RESUMEN

El Escudo Etíope Occidental está debajo de terrenos volcánicos sedimentarios, terrenos gneissicos y rocas ofiolíticas intruidas por diferentes cuerpos granitoides. El área Megele es parte del Escudo Etíope Occidental y consiste en una zona volcánica sedimentaria de bajo grado con intrusiones máficas (diques doleríticos) y granitoides (granodioritas, dioritas, granito gneissico). En este trabajo se realizaron caracterizaciones petrológicas, petrográficas y geoquímicas de estas rocas para establecer el origen de las litologías distintivas de la localidad y evaluar su potencial mineral. A partir de las caracterizaciones se ilustraron las características litológicas, geoquímicas y petrogenéticas de los granitoides intrusivos del Neoproterozoico y metavolcánicos asociados a través de una combinación de mapeo de campo y análisis petrológicos y geoquímicos. Los resultados petrológicos obtenidos del análisis de secciones delgadas de los granitoides y metabasaltos del área de Megele indican que estas rocas han presentado metamorfosis desde facies de esquistos bajos de color verde a facies de anfibolita, como lo denotan los grupos minerales albite + muscovita + prehnita + cuarzo y actinolita + hornblenda + epidota + granate. Los análisis geoquímicos de elementos mayores y traza de gneisses de granodiorita, diorita y granito revelaron que las rocas en el área de estudio son principalmente calcoalcalinas y peraluminosas, según los gráficos  $\text{SiO}_2$  frente a  $\text{Na}_2\text{O}+\text{K}_2\text{O}$  y A/NK frente a A/CNK. Los granitoides son granitos tipo S que revelan que las rocas saturadas de sílice se formaron en el arco volcánico de subducción, en un escenario tectónico syn-colisional por el fraccionamiento de magma basáltico enriquecido en tierras raras ligeras y mermado en tierras raras pesadas con una considerable aportación de la corteza. Este magma basáltico, al parecer, se generó en un manto enriquecido de tierras raras ligeras y mermado de tierras raras pesadas. En conclusión, el metabasalto es subalcalino (toleítico), y los cuerpos metaluminosos se generaron en un ambiente de dorsal mediooceánica al derretir parcialmente el magma basáltico mermado en tierras raras pesadas y enriquecido en tierras raras ligeras. Las fuentes magmáticas están asociadas con los bloques de corteza sedimentaria refundida de la zona de subducción y que produjeron granitoides tipo S.

**Palabras clave:** cristalización fraccionada; geoquímica; Megele; Neoproterozoico; petrogenesis; granitos tipo S.

### Record

Manuscript received: 04/11/2021

Accepted for publication: 23/06/2022

### How to cite item:

Oljira, T., Okunlola, O. A., Olatunji, A. S., Ayalew, D., & Bedada, B. A. (2022). Petrogenesis of the Neoproterozoic rocks of Megele area, Asosa, Western Ethiopia. *Earth Sciences Research Journal*, 26(2), 157-172. <https://doi.org/10.15446/esrj.v26n2.98451>

## 1. Introduction

In Ethiopia, different geological studies have confirmed the presence of different rock types of different origins, ages, and evolution, and associated mineralizations. The main rocks exposed widely in the country are mainly fall into three broad categories; the Neoproterozoic metamorphic rocks, Mesozoic sedimentary rocks, and Tertiary volcanic rocks (Asefa *et al.*, 1981). Among them, the Neoproterozoic basement complex is the largest rock suite exposed in northern, eastern, southern, and Western parts of Ethiopia (Fig. 1a). According to (Tadesse *et al.*, 2003) most economic metallic mineral deposits are known to be found in this Neoproterozoic basement complex, including precious metals like Au, Pt, PGE, Ni, Ta, base metals, industrial minerals, and gemstones (i.e., ruby, emerald, sapphire, garnet), and decorative dimension stones. Several studies suggested that the tectonic and thermal evolution of Ethiopia's Juvenile Neoproterozoic volcano-sedimentary terranes of low-grade metamorphic belts and associated granitoid intrusions is primarily responsible for these metallic and nonmetallic mineral resources (Tadesse *et al.*, 2003; Warkisa *et al.*, 2021). Even though the geology of Western Ethiopia is still not well understood, different studies have been conducted in the region from different perspectives. Western Ethiopian Shield is classified into Arabian Nubian Shield which comprises of Neoproterozoic low-grade metamorphic rocks and Mozambique belt includes moderate-to-high-grade gneisses (Kazmin, 1971; Kazmin *et al.*, 1978; Kebede *et al.*, 1999). Furthermore, detailed studies have been conducted in specific parts of the area focusing on geotectonic evolutions (Ayalew and Johnson 2002), petrology, geochemistry, and tectonic settings (Kebede *et al.*, 1999; Alemu and Abebe, 2007; Warkisa *et al.*, 2021). The Asosa area in the Western Ethiopian Shield which is the focus of this study has been one of the targeted areas for placer gold mining by artisanal workers since the 1930s (Bullock and Morgan, 2018). Based on the results of the field investigation, geological mapping and preliminary geochemical information (Bullock and Morgan, 2018) revealed that there has primary gold mineralization in shear zone related quartz veins, quartz-graphite schist, pegmatite, and quaternary basalts.

Furthermore, (Bullock and Morgan, 2018) reported that there is an association of gold with pyrite, chalcopyrite, galena, and with minor pyrrhotite, hematite, and graphite ores. However, the petrological, geochemical, and tectonic setting description of the Neoproterozoic rocks of the Megele area is yet unknown. Thus, using an integrated field relationship, Petrographical characteristics, major oxide, and trace elements interpretations induced the petrogenetic, geochemical and tectonic setting character of the Neoproterozoic metamorphic and granitoid intrusive rocks units from the study area (Megele area) of Western Ethiopian Shield.

## 2. Geological setting of Western Ethiopian Shield

East African orogeny (Stern, 1994) which is the largest continuous Neoproterozoic -Cambrian orogen (Fritz *et al.*, 2013) traditionally subdivided as Arabian Nubian Shield (ANS) in the north, comprising juvenile Neoproterozoic crust (Abdelsalam and Stern, 1996; Johnson *et al.*, 2011; Johnson and Woldehaimanot, 2003; Stern, 1994) and the Mozambique Belt (MB) in the south composed of pre-Neoproterozoic crust with tectonothermal overprint spanning from Neoproterozoic to early Cambrian (Bingen *et al.*, 2009; Collins, 2006; Fritz *et al.*, 2006; De Waele *et al.*, 2006). Western Ethiopian Shield is part of the East African Orogeny and is composed of Neoproterozoic low- to high-grade metamorphic and mafic-ultramafic rocks (Fig. 1). This Western Ethiopian Shield is the southern extension of two contemporaneous Pan African belts i.e., the Arabian Nubian Shield and Mozambique belt. Arabian Nubian Shield (ANS) is composed of Neoproterozoic low-grade volcano-sedimentary rock units whereas the Mozambique belt (MB) is made of high-grade gneiss and reworked continental crusts (Fig. 1). Both Neoproterozoic Arabian Nubian Shield and Mozambique belt metamorphic complexes are intruded with different generations of syn- to post granitoid intrusive rocks (Asrat and Barbey, 2003; Tadesse *et al.*, 2003). The Western Ethiopian Shield shows an inter-fingering of the high-grade gneisses and low-grade volcano-sedimentary rock units. They consist of Yubdo-Dalati-Tulu Dimtu ultramafic rocks belts which are correlated

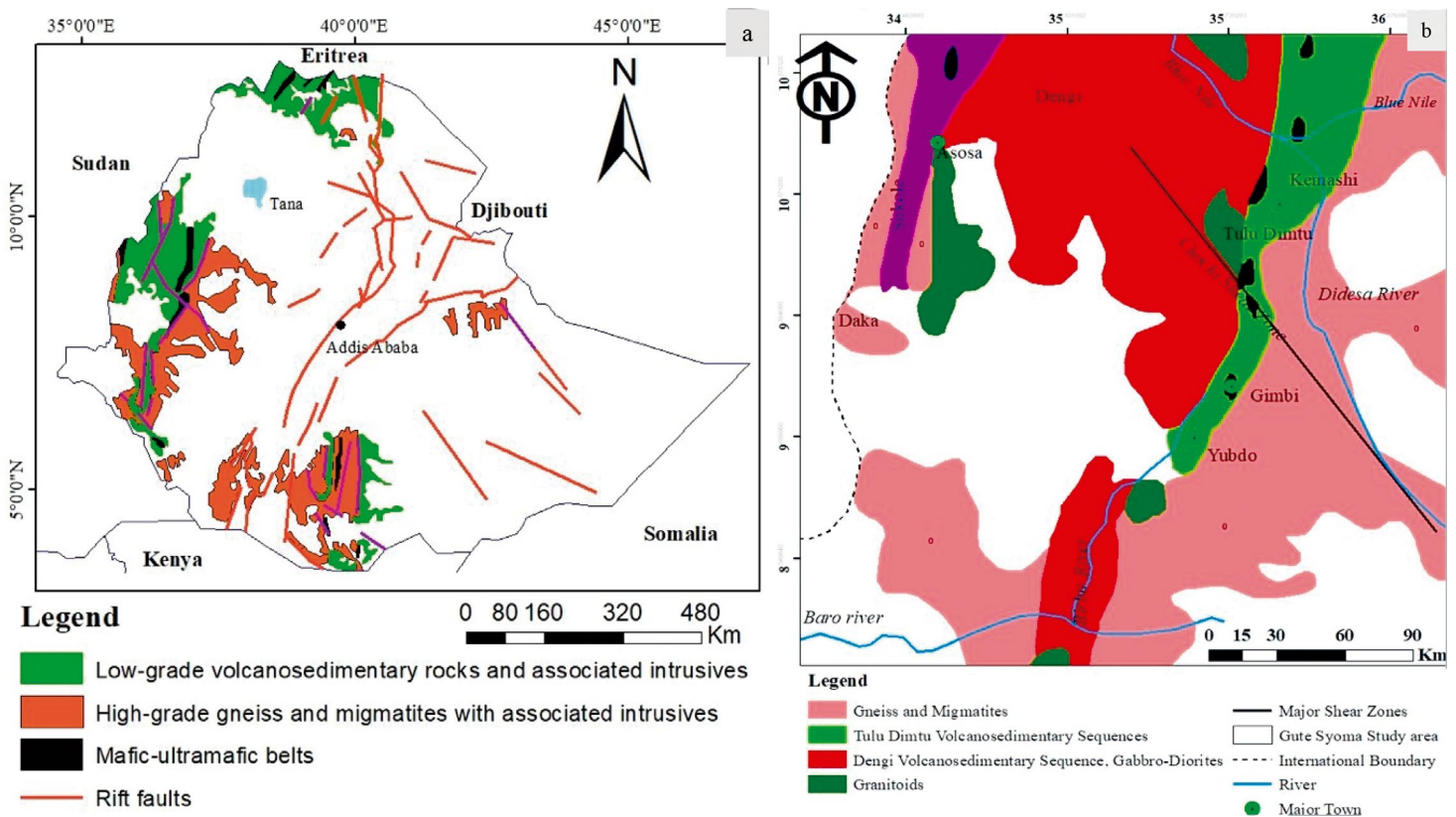


**Figure 1.** Map showing: (a) the distribution of the Neoproterozoic Pan-African belts (ANS and MB) and reworked Pre-Neoproterozoic crust in Ethiopia (modified after Asrat *et al.*, 2001) and (b) Western Ethiopian Shield in the vicinity of Megele area (after Allen and Tadesse, 2003).

to the Arabian Nubian Shield (Kebede *et al.*, 1999; Alemu and Abebe, 2007). According to (Blades *et al.*, 2015) the Arabian Nubian Shield Neoproterozoic basement complex is composed of a variety of supra-crustal and plutonic intrusive rocks that developed in the Tonian volcanic arc setting. The pre-, syn-, and post-tectonic plutonic intrusive rocks of varying composition have intruded the Arabian Nubian Shield of Western Ethiopian Neoproterozoic basement rocks (Warkisa *et al.*, 2021) (Warkisa *et al.*, 2021). In view of (Blades *et al.*, 2015, 2019; Warkisa *et al.*, 2021) the Western Ethiopian Shield is originated during the east and west Gondwana collision and evidence for a complete tectonic cycle, island-arc, and arc-accretion activities. As studied by (Ayalew, 1997; Ayalew *et al.*, 1990; Ayalew and Peccerillo, 1998) the Western Ethiopian Shield consists of Baro, Birbir, and Geba Domains (Fig. 1b). The lithotectonic rocks units of these domains are mainly developed in N-S, NNE-SSW, and slightly W-E orientations. Baro and Geba domains are comprised of quartzofeldspathic gneiss, biotite-hornblende gneiss, biotite gneiss, amphibolite facies, migmatites, and numerous subconcordant lenses of granitic-pegmatitic rocks units (Ayalew *et al.*, 1990; Ayalew and Peccerillo, 1998; Stern *et al.*, 2004; Wolde *et al.*, 1996). These rocks are characterized by medium to coarse-grained textures. The Birbir domain is extended to the Asosa region and confined between the Geba domain from the east and Baro domain from the Western direction. This domain is composed of low-grade meta-volcano sedimentary, mafic to felsic granitoid intrusions, volcanoclastic, and carbonate rocks. Later (Ayalew and Johnson, 2002) recognized that the Birbir domain rocks units which are fine-grained schists, metamorphosed to the lower amphibolite facies and exhibited primary sedimentary structures like bedding, cross lamination, and load-casts features. Further (Allen and Tadesse, 2003) classified Tuldumtu Ophiolitic Belt (TDB) (in the northern section of Western Ethiopian Shield) into Didesa domain, Kemashi domain, Dengi domain, Sirkole domain, and Daka domain from east to west using lithostratigraphic and structural similarities. Among these, the Kemashi, Dengi, and Sirkole Domains are largely comprised of Neoproterozoic low-grade volcano-sedimentary rocks, located in the central part of the Tuldumtu Ophiolitic Belt, enclosed from east and west by the Didesa and Daka Domains respectively (Fig. 1b) whereas the Didesa and Daka Domains are composed of Neoproterozoic high-grade gneissic rock units. The Kemashi Domain consists of an ophiolitic sequence such as mafic-ultramafic volcanic, plutonic, and sedimentary rocks of oceanic affinity, which evolved from oceanic crust at an arc-continent suture zone (Allen and Tadesse, 2003; Blades *et al.*, 2015). The Dengi Domain is made up of mafic to felsic intrusive, the succession of volcanoclastic, volcanogenic, and carbonate deposits that indicate a volcanic arc tectonic setting. As investigated by (Allen and Tadesse, 2003) Sirkole domain is characterized by an alternate layer of high-grade gneiss and low-grade volcano-sedimentary rock sections and which are thought to be part of an imbricated basement-cover thrust-nappe complex. The calc-alkaline metavolcanics intercalated with metasediments and intruded by calc-alkaline plutons underpin the central part of the Tuldumtu Ophiolitic Belt. Allen and Tadesse (2003) identified different generations of syn- and post-kinematic plutonic intrusion rocks in the Western Ethiopian Tuldumtu Neoproterozoic Ophiolitic rocks belt.

### 3. Sampling and analytical methods

An integrated field mapping, petrographical, and geochemical studies were conducted during this study. Totally 25 representative rock samples were collected from the study area (Megele) in the Sirkole Domain, Asosa, Western Ethiopia. The collected samples for analysis are representative and collected from insitu outcrop by breaking the inner rocks to maintain the freshness of the samples. Among the gathered samples, 25 rock samples (3 from Amphibole schist, 3 from Diorite, 5 from Granite gneiss, 3 from Granodiorite, 3 from Quartz graphite schist, 5 from Metabasalt, and 3 from Talc schist) were analyzed for petrographic study. While 21 fresh rock samples (3 from Amphibole schist, 2 from Diorite, 5 from Granite gneiss, 2 from Granodiorite, 2 from Quartz graphite schist, 5 from Metabasalt, and 2 from Talc schist) were analyzed for whole-rock geochemical study (Table 1). Thin sections were made at center for geoscience laboratory, geological survey of Ethiopia and studied at school of Earth science, Addis Ababa University, Ethiopia to decipher the texture, mineralogy, and to evaluate the degree of alteration. For whole-rock geochemical analysis, the selected samples were first dried, crushed, and pulverized at ALS global

services geochemistry laboratory, Addis Ababa, Ethiopia. The pulverized samples were then sent to the analytical testing service (ALS), Ireland for major, trace, and rare-earth elements analysis. Then, each pulverized sample of 0.2 gm is thoroughly mixed well with lithium metaborate/lithium tetraborate flux of 0.9 gm and ignited at 1000°C in a furnace (ALS, 2021). After cooling, the resultant melt is dissolved in 100 mL of a 4% (HNO<sub>3</sub>)/2% (HCl) solution. Then, ICP-MS (Agilent 7700) and ICP – AES (Agilent 5800) are used to examine the resultant solution for major oxide, trace elements including rare-earth elements (ALS, 2021). The analytical methods were selected bearing in mind their capacity to detect wide range of determinants in the all of the sample media at background level and as good as significantly better than the natural geochemical variations. The analytical precisions are estimated to be 2% for major elements, and 5% and 10% for trace element concentration higher or lower than 20 ppm respectively. The detection capacity of the selected methods ranges from 0.01% to 100% for major element and 0.01% to 10,000 ppm for trace elements. But for Cr and V, the detection capacity ranges from 10 to 10,000 ppm and 5 to 10,000 ppm respectively.

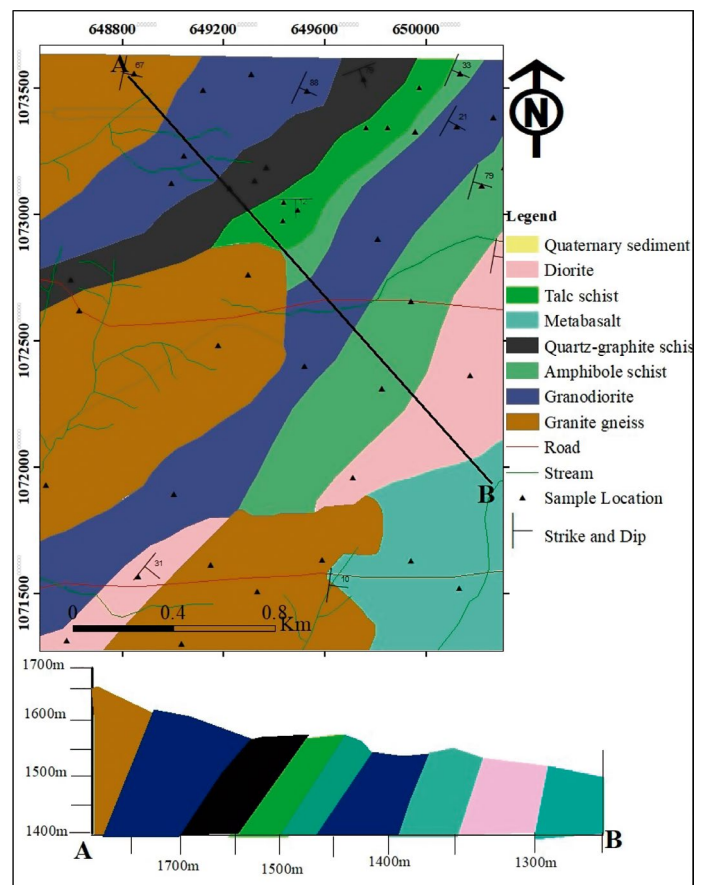
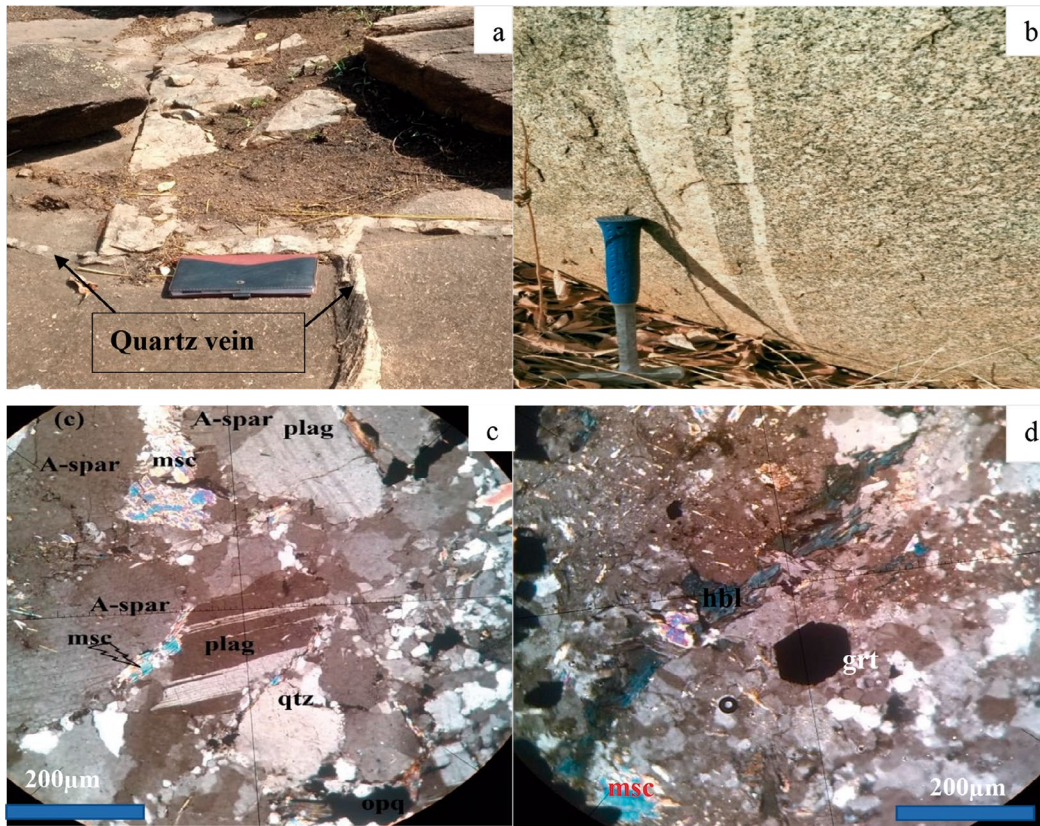


Figure 2. Map showing the detailed geological map of Megele area

## 4. Results

### 4.1. Local geology

The Megele area is characterized by the exposure of quartz-graphite schist, amphibole schist, talc schist, diorite, granite gneiss, metabasalt and granodiorite marked by mafic intrusions (dykes), quartz veins, and veinlets (Fig. 2). The general trend of the units in this locality is NNE-SSW. Specifically, the granite gneiss trends NNE-SSW and dips 48° north-eastward, while the talc schist dips 12° southward (Fig. 2). Using field exposure and microphotographs of thin sections, the major rock units are described below (Fig. 3-9).



**Figure 3.** Exposure of fractured granite gneiss filled with quartz vein (a and b); Microphotographs in XPL: (c) granite gneiss showing anhedral muscovite filling fracture within alkali feldspar, (d) euhedral garnet within alkaline minerals. Note: Bt-biotite, msc-muscovite, qtz-quartz, plag-plagioclase feldspar, A-spar, Alkali feldspar, hbl-hornblende, grt-garnet.

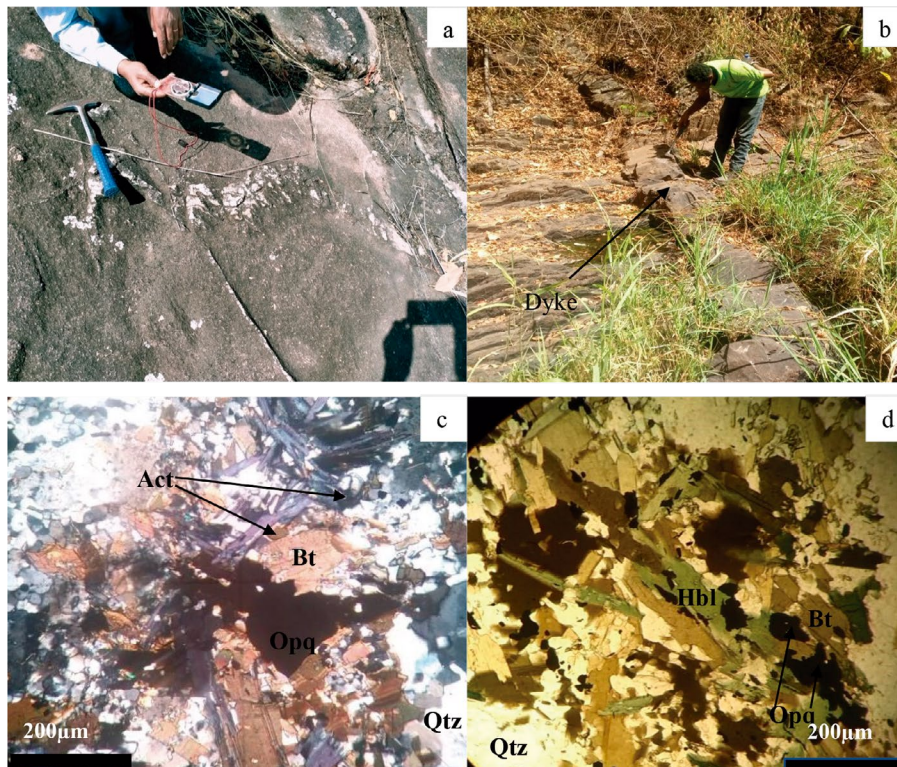


**Figure 4.** (a) Exposure of fractured granodiorite filled with quartz vein; (b) Dyke perpendicularly cutting the granodiorite; Microphotographs in XPL (c and d) anhedral opaque minerals within alkaline minerals. Note: Act-Actinolite, Bt-biotite, qtz-quartz, Opq-opaque

#### 4.1.1. Granite gneiss

The granite gneiss is the dominant unit in Megele area and makes a contact with granodiorite, diorite, talc schist, amphibole schist, quartz-graphite schist and metabasalt (Fig. 2). It dominantly appears light grey to grey and crops out everywhere forming mountains and plutonic plugs. The granite gneiss rock unit appears medium to coarse-grained textures and comprised of quartz, feldspars, and mica minerals. Large phenocrysts of black micas are occasionally observed throughout the rock and the color of the rock dominantly resumed the color imposed by the mica minerals. The granite gneiss has been fractured and the fracture has been filled by silica forming quartz veins (Fig. 3a, b). Locally, it has been fractured, weathered, and altered. In addition to silicification that is commonly observed in the rock especially, near the quartz veins and veinlets, the rock has also undergone sericitization and kaolinization, and epidotization. The petrographic descriptions reveal that the granite gneiss consists of euhedral quartz, alkali-feldspars, plagioclase, and other alteration minerals (Fig. 3c and d). The other observed alteration minerals are muscovite, garnet, chlorite, and hornblende. The most dominating minerals in the rock are feldspars orthoclase outclassing among them (Fig. 3a). The mineral constituents of the rocks are: K-feldspar (26%), quartz (29%), biotite (11%), plagioclase (9%), hornblende (17%), muscovite (5%), and opaque=3%. Some plagioclase (with polysynthetic twins), muscovite, and hornblende exist. In some of the plagioclase crystals, micro fracturing is observed showing the inclusion of quartz within the cracked part of the plagioclases. The muscovite in the sample is both primary and secondary. The hornblende appears greenish to brownish green and at some of its rim, there are opaque minerals which are probably magnetite that resulted from oxidation of Fe (Fig. 3d). Very rare sericite with grossular garnet inside it and biotite are other components that constituted the rock. Sericitization is interpreted as a process that involved in the alteration of k-feldspar enhanced by the presence of hydrothermal fluids. The rarely observed garnet in the rock shows fractures that might have resulted from compressional deformation that resulted in fracturing that is also visible at a larger scale in the field. The opaque minerals observed in the rock range between anhedral and euhedral crystal forms with some visible isometric and rhombohedra minerals. The fractured body and occurrence of low-grade metamorphic minerals indicate that the garnet in the rocks is primary. However, there are also secondary and/or grossular garnet grains that are characteristics of low-grade metamorphism of granitoid biotite.

#### 4.1.2. Granodiorite

The granodiorite, which makes contact with granite gneiss, diorite, quartz-graphite schist, and amphibole schist (Fig. 2). This rock unit is the second-largest rock unit in the study area. It is a massive to weakly foliated rock. It is a light to dark grey unit mainly composed of quartz, feldspars, and biotite (Fig. 4c, d). This unit has been intruded by basaltic dike perpendicular to the contacts and the regional foliation (Fig. 4b). The unit consists of multiple quartz veins. The field observation of this granodiorite unit shows the presence of plenty of visible phenocrysts of quartz and pyrite. The mineral constituents of the rocks are: Quartz (29%), Plagioclase (24%), alkaline-feldspar (10%) biotite (15%), garnet (3%), hornblende (4%), actinolite (6%), chlorite (6%), and opaque minerals (3%). The anhedral quartz minerals are dominant in the rocks followed by elongated plagioclase (Fig. 4c). While the hornblende and biotite are elongate and anhedral respectively in shape situated within the anhedral quartz (Fig. 4c, d).

#### 4.1.3. Diorite

The diorite unit in the study area cropped out around the Abuloshele area and bounded by granite gneiss, granodiorite from the southwest and by amphibole schist and metabasalt from the northeast (Fig. 2). It appears grey to dark-grey in color and it is composed of medium to coarse grain minerals with visible quartz, biotite, and pyroxene. In a similar fashion to granodiorite, the diorite unit has been cut by quartz veins of different orientation which resulted in an intense degree of silicification. Apart from silicification, the rock has also been subjected to chloritization, epidotization, and oxidization. The major oxide mineral in this unit and most of the units in the area is a brownish-black iron oxide, magnetite. Petrologically, it contains minerals like quartz (27%), plagioclase (21%), biotite (13%), hornblende (10%), and epidote (5%), chlorite (7%), actinolite (9%), garnet (4%), amphibole (2%), and opaque minerals (2%) (Fig. 5b, c, and d). The diorite thin section microphotograph (Fig. 5c) shows

anhedral biotite and muscovite segregating from anhedral quartz forming alignment; and euhedral garnet growth at the boundary of quartz, plagioclase and alkali feldspar (Fig. 5d).

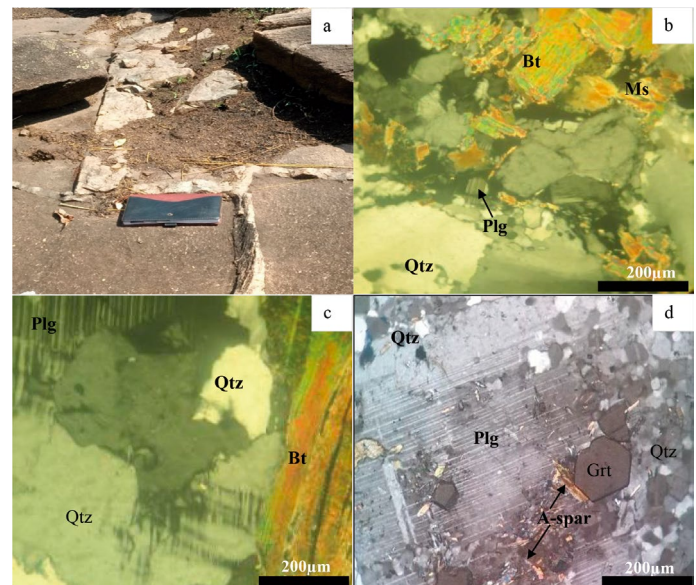


**Figure 5.** (a) Exposure of fractured diorite filled by two generation of quartz vein; Microphotographs in XPL of diorite (b and c) showing anhedral biotite and muscovite segregating from anhedral quartz forming alignment; and (d) euhedral garnet growth at the boundary of quartz, plagioclase and alkali feldspar. Note: Bt-biotite, Ms-muscovite, Plg-plagioclase, Qtz-quartz, A-spr: K-feldspar, Grt-garnet.

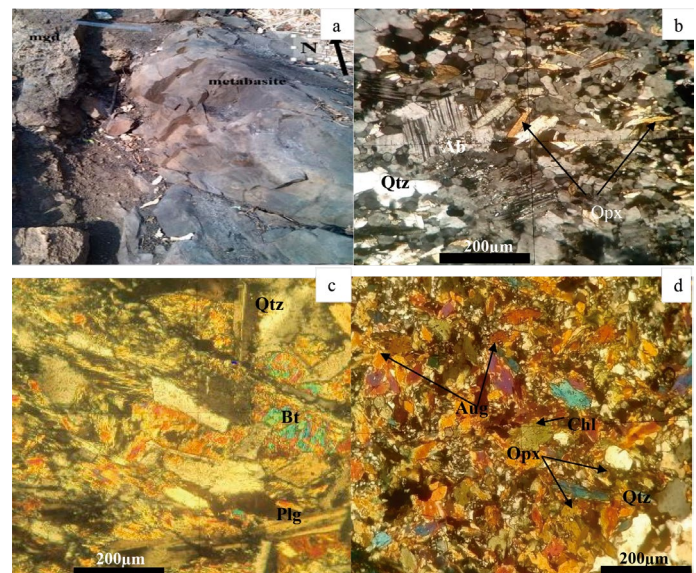


**Figure 6.** (a) Exposure of massif metabasalt; Microphotographs in XPL: (b) metabasalt showing platy orthopyroxene within anhedral quartz groundmass; (c) elongated plagioclase and (d) anhedral augite and chlorite evolving within alkaline minerals. Note: Aug-Augite, Bt-biotite, Chl-chlorite, ep-epidote, Plg-plagioclase, fsp-feldspar, Qtz-quartz, Opx-orthopyroxene.

#### 4.1.4. Metabasalt

The metavolcanic rock is exposed at the eastern section of the study area (Megele) in the Sirkole Domain, Western Ethiopia (Fig. 2). The rock unit appear greenish to dark color, show a sharp contact with the granite gneiss, and quartz-graphite schist where it can be observed. Degrees of chloritization and epidotization are much higher in this unit than in the others with moderate silicification. Silicification is relatively more intensely observed around the

quartz veins and veinlets within itself or where it contacts the intermediate rocks. This unit is the third-largest unit after granite gneiss and granodiorite in the area. The samples from metabasalt show porphyritic texture in a fine-grained, holocrystalline matrix under a thin section with plagioclases dominating among the phenocrysts. Mineralogically, the metabasalt is dominated by pyroxenes and plagioclases with minor chlorite, hornblende, and opaque minerals. The metabasalt in the area are of two different mineralogy. The first units consist of some amount of quartz (~4vol%), the other minerals including albite, chlorite, ortho-pyroxene, and no to very rare olivine. The other units have more mafic minerals like ortho-pyroxene, green amphibole, chlorite, and epidote than the formers with lesser quartz. The overall mineralogy of the metabasalt is: quartz (16%), pyroxene (13%), plagioclase (20%), biotite (10%), chlorite (6%), hornblende (11%), epidote (5%), amphibole (7%), alkali-feldspar (4%), prehnite (3%) and opaque minerals (5%) (Fig. 6b, c and d). The presence of rare prehnite in both metabasalt samples indicates sub-greenschist facies metamorphic grade. The photo micrographs of metabasalt shows platy orthopyroxene within anhedral quartz groundmass (Fig. 6b); elongated plagioclase (Fig. 6c) and anhedral augite and chlorite evolving within alkaline minerals (Fig. 6d).



**Figure 7.** Exposure: (a, b) Talc schist, and microphotographs: (c and d) Talc schist showing different minerals. Note: all microphotographs were taken in XPL. Tlc-talc, Mgs- magnesite. Most of this field of view is covered by talc

#### 4.1.5. Talc schist

This unit is a thin two to three-meter-thick Talc schist layer found between granodiorite and granite gneiss units (Fig. 2). It is characterized by a whitish color and slightly foliated. This unit is exposed around Yohotse and Korondo rivers. It has sharp contact with surrounding granodiorite units. From the petrographic analysis the rock is composed of 60% talc, 20% magnesite, 15% actinolite and 5% opaque (Fig. 7c and d). Talc, magnesite and opaque minerals show well developed parallel alignment and they define strong foliation for this thin section. This thin section displays schistose texture.

#### 4.1.6. Quartz-Graphite schist

Extensive quartz-graphite is observed around the Abuloshele, Korondo, and Yohotse river trending NNE-SSW direction in the area (Fig. 2). This unit is sandwiched between granodiorite to the west and granite gneiss and amphibole schist to the east and north east respectively (Fig. 2). The quartz-graphite schist unit appears grey and shows carbonization alteration. Thin section of this rock unit contains 51% graphite, 35% quartz, 9% muscovite (sericite) and 5% biotite (Fig. 8c, d). Quartz, graphite, micaceous (sericite), opaque and biotite show strong parallel alignment and they define strong foliation as a result the thin section show schistose texture. Quartz and graphite display xenoblastic texture, muscovite (sericite) display tiny platy and biotite displays flaky.

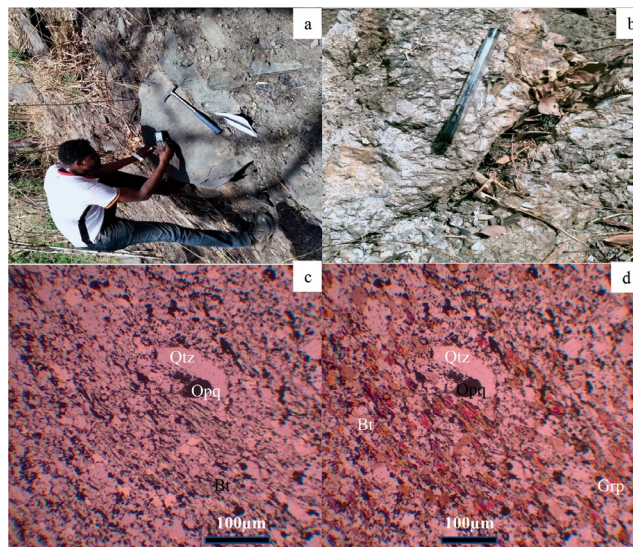


**Figure 8.** Exposure: (a) Quartz-graphite schist, (b) thick quartz vein; microphotographs (c, d) of quartz-graphite schist showing different minerals: Note: microphotographs (c) taken in PPL while (d) were taken in XPL. Qtz-Quartz, Gpr-Graphite, Bt-Biotite, Opq-Opaque. Note: parallel alignment of minerals suggesting schistose texture.

#### 4.1.7. Amphibole schist

This unit is a thin two to three-meter-thick amphibole schist layer found bounded by diorite in the east and granodiorite and talc schist units in the northwest (Fig. 2). The amphibole schist is dark green, slightly foliated massive units in place (Fig. 9a, b). This unit is exposed in Yohotse and Korondo rivers. It has sharp contact with surrounding units and striking NNE and dips at 47° south-eastward. The mineralogical constituent of this rock is: quartz (25%), hornblende (21%), muscovite/sericite (14%), actinolite (13%), chlorite (10%), epidote (7%), biotite (9%), plagioclase (6%), and opaque 5% (Fig. 9c, d). Minerals like biotite, chlorite, hornblende and muscovite (sericite) show well developed parallel alignment of schistosity. Hornblende altered to chlorite and Biotite replaced by chlorite. Quartz crystals are strained due to deformation

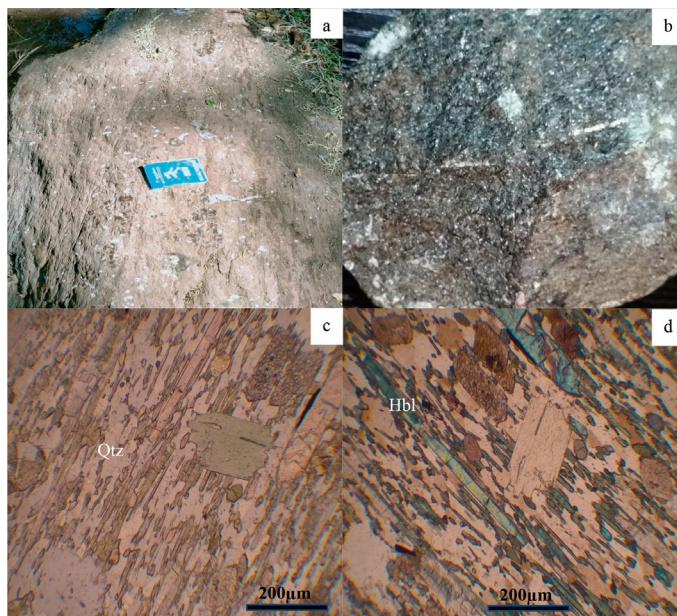


**Figure 9.** Exposure: (a) Amphibole schist, and microphotographs (c in PPL and d in XPL): Amphibole schist showing different minerals. Qtz-Quartz, Hbl-Hornblende, Chl-Chlorite.



**Figure 10.** Field photograph showing Quartz veins of different orientation



**Figure 11.** Field photograph showing mafic dyke cutting the granodiorite layer

#### 4.1.8. Quartz vein

The quartz vein in the Megele area are distributed through granitoids, diorite, granodiorite, and graphite schist units. They show two general trends; nearly E-W and N-S trending veins and most of them are long in their strike direction and possess varying width ranging from 5 cm to 3 m. At some localities, the quartz veins of different orientations cross one another and leave the N-S oriented ones displaced (Fig. 10a, b, c, d). The displacement of these N-S oriented quartz veins when they are cut by the E-W oriented veins infers that the formers are formed earlier. The displacement of the N-S oriented quartz veins was caused by the creation of fractures in the E-W oriented veins, which were then filled with hydrothermal fluid concentrations. In the study area, a few of the quartz veins are randomly oriented and lack continuity. These quartz veins are believed to be metamorphic in their origin and precipitated in deformational openings related to metamorphism.

#### 4.1.9. The Mafic Dyke

The mafic (basaltic) intrusive bodies of varying thicknesses which range from 10 to 50cm intrude the granodiorite (Fig. 11). These dykes are oriented

E-W and NNW-SSE and they are perpendicular to both the contact between the meta- granodiorite and granite gneiss and the regional foliations.

#### 4.2. Geochemistry

The whole-rock geochemical analytical results for major oxides and trace elements including rare-earth elements are presented in (Table 1). The selected whole-rocks samples are affected by significant hydrothermal alterations such as epidotization, chloritization carbonization, sericitization, silicification, pyritization, and oxidation and mineralization. It is probably due to these alteration effects that these analyzed rock samples show results less than 100 wt% total of the oxides (which is ~99 wt% in altered granite gneiss, metabasalt, and granodiorite and as low as ~98wt % in the graphite schist). In the Harker variation graphs, however, certain distinct geochemical trends can be seen (Fig. 10).

Table 1. Whole-rock geochemical analysis result for selected Neoproterozoic rocks of Megele area: major oxides (wt%) and trace and RE element (ppm)

Rock Name	Granodiorite		Quartz Graphite schist		Talc schist		Metabasalt				
Sample Code	ATP-GD1	ATP-Gd2	ATP-Gp-1	ATP-Gp2	ATP-T1	ATP-T2	ATP-MB1	ATP-MB2	ATP-MB3	ATP-MB4	ATP-MB6
<b>Major elements wt%</b>											
SiO <sub>2</sub>	60	55.8	85.7	82.1	78.6	76.6	54.7	54.4	56.8	56	52.9
Al <sub>2</sub> O <sub>3</sub>	17.1	18.8	5.54	5.17	12.8	13.1	17.3	17.1	15.75	15.15	6.18
Fe <sub>2</sub> O <sub>3</sub>	6.75	6.66	3.04	2.29	2.32	2.8	2.3	2.27	10.4	11.75	5.06
CaO	2.61	2.76	0.04	0.05	0.02	0.02	0.38	0.35	5.82	6.35	0.03
MgO	3.06	2.91	0.11	0.15	0.69	0.71	0.09	0.05	4.94	6.2	0.1
Na <sub>2</sub> O	4.35	5.87	0.26	0.24	0.13	0.14	10.6	10.45	4	3.33	0.24
K <sub>2</sub> O	1.82	1.84	0.87	1.19	4.2	4.24	5.16	5.17	0.51	0.13	0.86
TiO <sub>2</sub>	0.97	1.08	0.31	0.35	0.35	0.35	0.21	0.21	0.29	0.34	0.31
MnO	0.07	0.07	0.01	0.03	0.02	0.02	0.23	0.23	0.18	0.19	0.03
P <sub>2</sub> O <sub>5</sub>	0.35	0.43	0.03	0.03	0.01	0.01	0.1	0.09	0.07	0.06	0.03
LOI	3.24	3.08	4.32	6.14	2.14	2.01	5.31	5.09	1.52	1.24	4.65
Total	100.32	99.3	100.23	97.74	101.28	100	96.38	95.41	100.28	100.74	70.39
<b>Trace elements (ppm)</b>											
Ba	834	812	1455	2020	1350	1320	37.1	29.7	53.6	65.4	1405
Ce	60.2	53.9	28.9	38.4	13.3	11.8	73.4	62.8	15.5	7.8	35.5
Cr	50	50	240	330	20	20	20	10	30	50	290
Cs	0.73	0.76	0.89	1.21	0.71	0.82	2.49	2.26	0.66	0.74	0.99
Dy	4.18	4.56	6.94	5.95	2.7	2.45	4.67	4.16	1.68	1.44	6.67
Er	2.4	2.5	5.16	4.75	2.14	2.27	2.87	2.71	1.24	0.9	4.22
Eu	1.51	1.69	1.12	1.07	0.32	0.2	1.38	1.29	0.48	0.31	0.98
Ga	18.8	19	9.3	9.4	16.3	16.8	46.7	41	15.1	14.2	9.9
Gd	5.66	5.74	7	6.23	1.84	1.66	4.28	4.24	1.54	1.21	6.4
Hf	4.6	4.4	2.4	2.6	7.8	8.1	24.7	22.4	2.4	0.6	2.2
Ho	0.86	0.97	1.78	1.53	0.66	0.64	0.93	0.82	0.43	0.32	1.51
La	31	26.8	25.8	29.7	7.4	6.9	35.2	29.2	7.5	4.2	27.2
Lu	0.41	0.39	0.78	0.71	0.51	0.57	0.55	0.48	0.2	0.21	0.64
Nb	8.6	9.8	4.7	5.8	14.9	15.1	432	384	35.7	1.9	4.8
Nd	28.5	26.9	22.3	26.6	6.9	6.5	25.1	22.5	6.5	3.7	23.4
Pr	7.15	6.61	5.34	6.16	1.66	1.66	7.75	6.9	1.71	0.96	5.57
Rb	38.4	35.7	32.5	37.1	73.7	73.7	197	172	15.7	2	31.9
Sm	5.53	5.29	4.7	4.63	1.39	1.52	4.65	4.13	1.4	0.95	4.65
Sn	2	2	3	1	3	2	3	2	1	1	2
Sr	363	377	188.5	109	47	47.3	60.4	51.9	224	235	167
Ta	0.5	0.5	0.2	0.1	0.6	0.6	27.4	24.1	2.8	0.1	0.1
Tb	0.69	0.74	1.09	0.91	0.41	0.34	0.74	0.68	0.27	0.18	0.92
Th	5.82	6.12	3.87	5.09	2.2	2.22	27.2	24.5	2.9	0.64	4.91
Tm	0.42	0.42	0.79	0.7	0.46	0.37	0.44	0.48	0.18	0.14	0.65

Rock Name	Granodiorite		Quartz Graphite schist		Talc schist		Metabasalt				
	ATP-GD1	ATP-Gd2	ATP-Gp-1	ATP-Gp2	ATP-T1	ATP-T2	ATP-MB1	ATP-MB2	ATP-MB3	ATP-MB4	ATP-MB6
U	2.17	2.39	2.48	2.41	2.79	2.59	9.5	8.48	1	0.19	2.32
V	156	150	321	366	16	11	7	8	237	286	352
W	3	5	4	1	3	2	3	2	1	2	6
Y	23.8	26.6	64.3	56.8	20.6	20	28.2	24.7	10.7	9.1	52.8
Yb	2.4	2.44	5.06	5.11	3.03	3.07	3.64	2.94	1.27	1.18	4.09
Zr	172	181	100	104	314	317	1300	1130	120	23	94
Cd	0.5	0.5	0.5	0.5	0.5	0.5	0.5	0.5	0.5	0.5	0.5
Co	26	24	1	1	1	1	1	1	26	34	1
Cu	6	3	22	2	7	6	1	1	131	125	12
Li	10	10	10	10	10	10	30	30	20	20	10
Mo	1	1	4	1	2	2	3	4	1	1	8
Ni	14	12	7	2	9	1	1	1	9	17	18
Pb	10	10	9	7	5	5	2	2	2	3	8
Sc	11	13	9	8	5	5	1	1	34	38	9
Ti	10	10	10	10	10	10	10	10	10	10	10
Zn	49	51	9	2	20	20	162	171	93	95	25
∑REE	150.99	139.03	116.17	131.85	42.86	40.18	192.56	166.95	42.52	23.46	122.54

Rock Name	Amphibole Schist			Granite					Diorite	
	ATP-AMB5	ATP-AMB7	ATP-AMB8	ATP-G1	ATP-G2	ATP-G3	ATP-G4	ATP-G5	ATP-G03	ATP-G04
<b>Major elements wt%</b>										
SiO <sub>2</sub>	48.5	45	45.3	72.9	73.2	71.7	72.9	72.9	55.5	58.7
Al <sub>2</sub> O <sub>3</sub>	10.7	10.5	10.4	14.1	13.7	14.95	15.3	15.15	42.7	39.4
Fe <sub>2</sub> O <sub>3</sub>	15.2	14.8	15	3.38	2.85	2.8	2.68	2.16	0.9	0.66
CaO	9.89	12.95	13.2	1.78	1.55	0.51	0.56	0.46	0.04	0.03
MgO	9.28	10.4	10.3	0.51	0.46	0.57	0.57	0.57	0.02	0.02
Na <sub>2</sub> O	2.05	0.69	0.68	3.52	3.07	4.66	4.74	4.69	0.64	0.49
K <sub>2</sub> O	0.16	0.21	0.19	4.35	4.89	2.96	3.07	3	0.16	0.14
TiO <sub>2</sub>	1.97	1.59	1.64	0.31	0.29	0.27	0.27	0.27	0.01	0.005
MnO	0.31	0.16	0.17	0.05	0.05	0.03	0.03	0.02	0.01	0.01
P <sub>2</sub> O <sub>5</sub>	0.03	0.15	0.16	0.12	0.1	0.09	0.09	0.08	0.01	0.01
LOI	1.53	2.72	2.63	0.76	0.94	1.24	1.39	1.23	1.12	1.18
Total	99.62	99.17	99.67	101.78	101.1	99.78	101.6	100.53	101.11	100.645
<b>Trace elements (ppm)</b>										
Ba	25	14	28.5	916	1300	1155	1220	1125	25	26.1
Ce	26	16.2	16.2	43	64.1	49	50.9	47.8	20.8	16.5
Cr	140	920	950	20	20	30	30	30	40	40
Cs	0.01	0.01	0.01	1.73	1.28	0.46	0.56	0.43	0.33	0.31

Rock Name	Amphibole Schist			Granite					Diorite	
Sample Code	ATP-AMB5	ATP-AMB7	ATP-AMB8	ATP-G1	ATP-G2	ATP-G3	ATP-G4	ATP-G5	ATP-G03	ATP-G04
Dy	4.99	3.32	3.33	3.27	3.74	1.1	0.95	0.95	3.6	3.27
Er	2.88	1.66	2	1.9	2.55	0.38	0.37	0.54	1.72	1.58
Eu	1.47	1.07	0.98	0.8	0.99	0.71	0.6	0.72	0.27	0.21
Ga	16.1	20	19.4	17.6	16.3	21.4	21.2	20.9	28.5	26.7
Gd	5.6	4.21	4.08	3.78	4.81	1.78	2.08	1.68	4.15	3.64
Hf	3.6	2.5	2.5	4.9	4.7	4	4	3.7	2.5	3.1
Ho	1.09	0.64	0.69	0.68	0.81	0.16	0.17	0.15	0.64	0.59
La	11.6	6.7	6.8	17	41.4	31.8	32.1	28.1	9.4	7.5
Lu	0.42	0.19	0.23	0.37	0.36	0.06	0.06	0.06	0.24	0.26
Nb	7.1	6.5	7.8	7.4	6.1	3.8	3.7	3.4	0.7	0.8
Nd	16.3	11.5	11.2	16	30.2	18.9	17.8	17.4	11.6	9.5
Pr	3.55	2.31	2.35	4.21	8.38	5.27	5.26	5	2.96	2.38
Rb	1.1	1.5	1.1	99.8	100.5	60.2	62.2	60.4	11.5	10.3
Sm	4.39	3.39	2.87	3.74	5.1	2.86	2.59	2.7	3.54	3.45
Sn	1	1	1	3	2	1	1	1	1	1
Sr	226	123	128.5	143	161.5	408	408	388	10.4	11.3
Ta	0.1	0.1	0.1	0.1	0.1	0.1	0.1	0.1	0.7	0.5
Tb	0.89	0.57	0.6	0.59	0.65	0.18	0.22	0.21	0.67	0.6
Th	0.97	0.44	0.51	6.75	6.09	5.99	5.89	6.27	4.14	3.57
Tm	0.45	0.24	0.28	0.33	0.36	0.04	0.04	0.02	0.22	0.21
U	0.35	0.15	0.14	1.34	0.92	1.44	1.5	1.5	1.79	2.17
V	283	220	247	25	25	24	27	26	118	122
W	2	4	4	2	2	3	1	2	3	3
Y	27.3	17	18.9	20	23.5	5	5.2	4.7	21.8	19.5
Yb	2.66	1.49	1.43	2.22	2.44	0.39	0.32	0.28	1.87	1.57
Zr	143	89	94	187	174	157	156	159	28	30
Cd	0.5	0.5	0.5	0.5	0.5	0.5	0.5	0.5	0.5	0.5
Co	57	81	78	2	4	2	2	2	1	1
Cu	1	66	119	7	5	12	14	22	4	2
Li	10	10	10	30	30	10	10	10	80	70
Mo	7	1	1	1	1	1	1	1	1	1
Ni	92	696	693	4	1	7	7	6	1	2
Pb	3	2	2	16	12	11	10	8	2	4
Sc	41	24	24	4	4	2	2	2	1	1
Ti	10	10	10	10	10	10	10	10	10	10
Zn	138	106	105	46	39	40	39	40	2	2
ΣREE	81.94	55.21	54.67	101.88	169.52	116.53	117.35	109.24	64.02	54.06

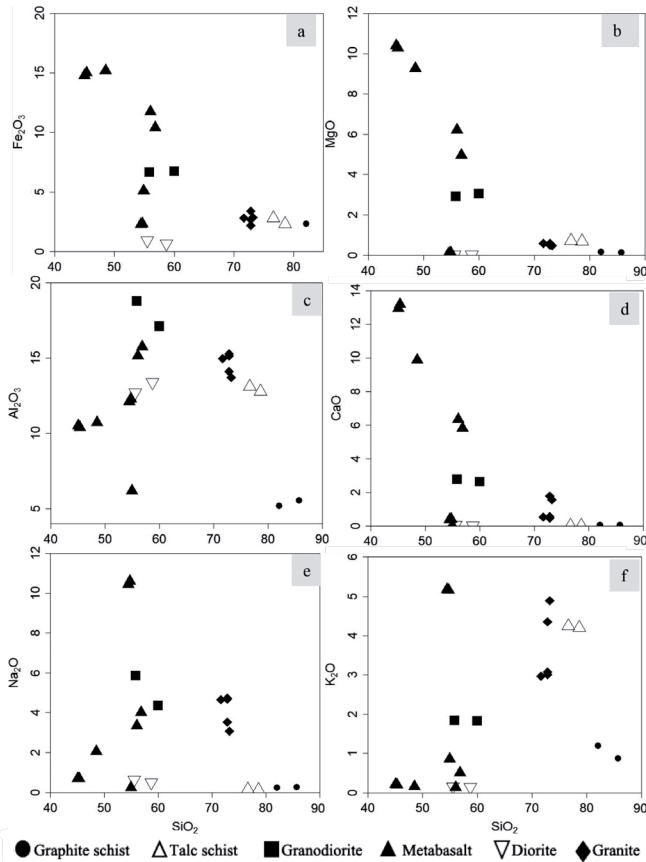


**Figure 12.** Harker variation diagram for major oxides of the Megele area Neoproterozoic rocks: (a) SiO<sub>2</sub> vs. Fe<sub>2</sub>O<sub>3</sub>; (b) SiO<sub>2</sub> vs. MgO; (c) SiO<sub>2</sub> vs. Al<sub>2</sub>O<sub>3</sub>; d) SiO<sub>2</sub> vs. CaO; (e) SiO<sub>2</sub> vs. Na<sub>2</sub>O; and (f) SiO<sub>2</sub> vs. K<sub>2</sub>O.

The granite gneiss samples have a major oxides concentrations for SiO<sub>2</sub> (71.7-73.2 Wt. %), Al<sub>2</sub>O<sub>3</sub> (13.7- 15.3 Wt. %), Fe<sub>2</sub>O<sub>3</sub> (2.42 Wt. %), CaO (0.48-1.78 Wt. %), Na<sub>2</sub>O (3-4.69 Wt. %), K<sub>2</sub>O (2.96-4.89 Wt. %), and (<1 Wt. % each) for MgO, TiO<sub>2</sub>, MnO, and P<sub>2</sub>O<sub>5</sub> (Table 1). The concentrations values of Fe<sub>2</sub>O<sub>3</sub>, MgO, P<sub>2</sub>O<sub>5</sub>, and MnO decrease with increasing SiO<sub>2</sub>, while the SiO<sub>2</sub> increases with increasing in Al<sub>2</sub>O<sub>3</sub>, Na<sub>2</sub>O, K<sub>2</sub>O, and CaO (Fig. 12). Trace elements including rare earth elements like Ba, Sr, and Rb increases with increasing SiO<sub>2</sub> (Table 1). The chondrite-normalized REE pattern for granite gneisses (Fig. 16a, b) plot to the values of (Nakamura, 1974) showed depletion of HREE relative to LREE and a negative Eu anomaly. The primitive mantle-normalized plot of (Sun and McDonough, 1989) revealed decreasing concentration of Nb, Sr, P, Ce, Eu, Ti, weak trough at Nd and Zr, and weak enrichment peaks at Ba, K, Pb (Fig. 16c, d).

The major oxides concentrations of diorite rock ranges from SiO<sub>2</sub> (55.5–58.7 Wt. %), Al<sub>2</sub>O<sub>3</sub> (12–14 Wt. %), Fe<sub>2</sub>O<sub>3</sub> (2–12 Wt. %), CaO (7–9 Wt. %), MgO (4–5 Wt. %), TiO<sub>2</sub> (>1 Wt. %), proportional K<sub>2</sub>O and Na<sub>2</sub>O contents (2–3 Wt. % each), and very low (<1 Wt. % each) MnO and P<sub>2</sub>O<sub>5</sub> contents (Table 1). As SiO<sub>2</sub> concentration increase the Fe<sub>2</sub>O<sub>3</sub>, and MgO concentrations decreases, while Al<sub>2</sub>O<sub>3</sub>, Na<sub>2</sub>O, K<sub>2</sub>O, CaO, TiO<sub>2</sub>, and P<sub>2</sub>O<sub>5</sub> concentrations are increasing (Fig. 12). The chondrite-normalized REE pattern for diorite plot to the values of (Nakamura, 1974) shows enrichment in LREE relative to HREE and a negative Eu anomaly (Fig. 16a, b). The primitive mantle-normalized plot of (Sun and McDonough, 1989) show a strong depletion in Ba, Nb, Sr, Ti, and P with a weak trough at Pb and U (Fig. 16c, d).

The granodiorite samples have SiO<sub>2</sub> range of 55.8-60 wt %, high Al<sub>2</sub>O<sub>3</sub> (17.1-18.8 wt %), high Fe<sub>2</sub>O<sub>3</sub> (~6.7wt %), MgO (~2.98 wt %), CaO (~2.66 wt %), Na<sub>2</sub>O (4.35-5.87 wt %), low K<sub>2</sub>O (~1.83 wt %), TiO<sub>2</sub> (~1 wt %), while MnO and P<sub>2</sub>O<sub>5</sub> show very low (<1 Wt. % each) concentrations (Table

1). The concentrations of Fe<sub>2</sub>O<sub>3</sub> and MgO decrease with increasing SiO<sub>2</sub> while the concentrations of Al<sub>2</sub>O<sub>3</sub>, Na<sub>2</sub>O, K<sub>2</sub>O, CaO, TiO<sub>2</sub>, and P<sub>2</sub>O<sub>5</sub> increase with increasing SiO<sub>2</sub> (Fig. 12). The chondrite-normalized REE pattern for granodiorite plot to the values of (Nakamura, 1974) indicates depletion of HREE relative to LREE and shows a negative Eu anomaly (Fig. 16a, b). The granodiorite trace elements primitive mantle-normalized plot of (Sun and McDonough, 1989), show decreasing Nb, Sr, P, Ce, Eu, Ti concentration with a weak trough at Nd, Zr and reveal weak enrichment peaks of Ba, K, and Pb (Fig. 16c, d).

The metabasalt samples have a SiO<sub>2</sub> range of 45-56.8 wt %, a high range of Al<sub>2</sub>O<sub>3</sub> (10.4-17.3 wt %), a low high range of Fe<sub>2</sub>O<sub>3</sub> (2.27-15.2 wt %), high range of CaO (0.38–13.2 wt %), high range of Na<sub>2</sub>O (0.68-10.6 wt %), high range of K<sub>2</sub>O (0.13–5.17wt%), TiO<sub>2</sub> (0.21-1.97 wt %), and minor concentration of MnO and P<sub>2</sub>O<sub>5</sub> (<1 wt % each) (Table 1). The concentrations of Fe<sub>2</sub>O<sub>3</sub>, MgO, CaO, and TiO<sub>2</sub> decrease with increasing SiO<sub>2</sub> while the concentrations of Al<sub>2</sub>O<sub>3</sub>, Na<sub>2</sub>O, and K<sub>2</sub>O increase with increasing SiO<sub>2</sub> (Fig. 12). The chondrite-normalized REE diagram for metabasalt (Fig. 16b) normalized plot to values of (Nakamura, 1974) shows slight enrichment in LREE relative to HREE with a negative Eu anomaly. The primitive NMORB plot (Fig. 16d) normalized to the values of (Sun and McDonough, 1989), show a strong depletion in Ba, Ti, and P (ATP-MB1, ATP-MB2, and ATP-MB5), weak crest at Nb, and Cs (ATP-MB4 and ATP-MB5) with a weak trough at Nb, Rb and Zr (ATP-MB7 and ATP-MB8).

The quartz-graphite schist samples have a range of SiO<sub>2</sub> (82.1-85.7 wt %), Al<sub>2</sub>O<sub>3</sub> (~5.35 wt %), low range of Fe<sub>2</sub>O<sub>3</sub> (2.29-3.04 wt %). While the concentration of CaO, MgO, Na<sub>2</sub>O, K<sub>2</sub>O, TiO<sub>2</sub>, MnO and P<sub>2</sub>O<sub>5</sub> is very low (<1 wt % each) (Table 1) in this rock unit. The concentration of Ba and Sr decreases with increasing concentration of SiO<sub>2</sub>. The Talc schist samples have a range of SiO<sub>2</sub> (76.6-78.6 wt %), Al<sub>2</sub>O<sub>3</sub> (~13 wt %), low Fe<sub>2</sub>O<sub>3</sub> (~2.3 wt %), K<sub>2</sub>O (~4.22 wt%), with very low concentration of CaO, MgO, Na<sub>2</sub>O, TiO<sub>2</sub>, MnO and P<sub>2</sub>O<sub>5</sub> (<1 wt % each) (Table 1).

## 5. Discussion

### 5.1 Petrography and metamorphism

The Neoproterozoic rocks and associated intrusive of Megele area comprise granite gneiss, granodiorite, metabasalt, diorites, and genetically linked quartz-graphite schists (Amena *et al.*, 2016; Bullock and Morgan, 2015; Bullock and Morgan, 2018). Granodiorite and granite gneiss intrusions were cut by different generations of the mafic dolerite dykes. Quartzo-feldspathic minerals are partially segregated from magnetite-biotitic minerals mainly in the sheared and altered domains of the granite gneiss and granodiorite unit. Amphiboles and biotite mineral grains show elongated and preferred orientation of foliations in the diorite, granite gneiss, and granodiorite units. The biotite-magnetite alteration is linked with the most deformed sections of diorite, granite gneiss, and granodiorite suggesting earliest alteration events in Megele area (Bullock and Morgan, 2015; Amena *et al.*, 2016). The secondary muscovite is commonly observed in association with the feldspars inferring replacement of the feldspars by muscovite due to alteration. This suggests the earliest alteration event in the Megele area. In granitoid rocks, even though the dominance of minerals that can occur in the wide range of temperature and pressure conditions makes it difficult to understand the grade of metamorphism, the field-based and petrographic study of the rocks shows that they were subjected to low to medium-grade of metamorphism. Some researchers like (Tulloch, 1979) used the existence of secondary minerals like minor Prehnite, andradite-grossular garnet, and epidote to infer that the granitoids underwent low-grade metamorphism and alteration products of granitoid biotite. The other metamorphic mineral that shows metamorphism of the granitoids of Megele area Neoproterozoic rocks is fibrous actinolite which occurs in association with biotite and other mafic minerals (like hornblende and actinolite). This mineral is commonly observed in granodiorite than in granite gneiss suggesting it is a product of alteration of mafic minerals. Prehnite is observed as lenticular to the bulbous body within mafic minerals like biotite, secondary chlorite, and hornblende in the metagranitoids. Their association with biotite indicates that they are metamorphic products replacing primary biotite (Tulloch, 1979). The presence of these minerals in the assemblage is an indication of low-temperature metamorphism which is also expected in other parts of the Western

Ethiopian shield as the area is believed to be a collisional and accretion zone. Generally, the established mineral assemblages for granitoids of Megele area are shown as: Prh + Act + Msc + Bt + Ab + Grt + Hbl + Qtz + kfs. The presence of prehnite (minor), actinolite, albite, and biotite in the assemblage reflects that the metamorphism took place in greenschist facies where low temperature-moderate pressure conditions existed. The mafic/andesitic metavolcanics (metabasalt) of the area also underwent a low to medium-grade metamorphic process. The presence of mafic minerals like prehnite which are characteristic of greenschist facies indicating metamorphism at low temperature and pressure. The presence of albite indicates dynamic environment thereby suggesting low-grade regional metamorphism. The metabasalt of the Megele area is characterized by mineral assemblage: Prh + Ab + Act + Opx + Aug + Qtz + Amp (Warkisa *et al.*, 2021).

### 5.2 Petrochemistry

The result of major oxides was interpreted to elucidate the petrogenetic characteristics of the Neoproterozoic rocks of the Megele area. In granodiorite and quartz veins, the  $\text{Fe}_2\text{O}_3$ ,  $\text{MgO}$ , and  $\text{CaO}$  contents decrease as silica increases (Fig. 12), implying fractionation of plagioclase and other mafic minerals during the course of magmatic differentiation and hydrothermal alteration process (Rollinson, 1993). On the other hand,  $\text{K}_2\text{O}$  and  $\text{Na}_2\text{O}$  is characterized by decreasing pattern for granite gneiss, granodiorite, diorite, talc schist and quartz-graphite schist, while it shows increasing pattern for metabasalt on the same silica fractionation line, supporting feldspar fractionation during hydrothermal alteration. Others (Asrat and Barbey, 2003; Ayalew and Peccerillo, 1998) revealed that in a subduction environment, basaltic magma generated from mantle start magmatic evolution by crystallizing Ca-rich plagioclase. This basaltic magma continues to fractionate more as the magma continue mixing with fluids generated from hydrothermal and wall rock assimilation Na-rich plagioclase as it cooled. From the TAS diagram after Cox *et al.*, (1979), as shown in fig. 13a, the granite gneiss of the studied area plot as granites, whereas the granodiorite and diorite samples plot as diorite. Also, the metabasalt plot in the diorite, gabbro and nepheline syenite field. This suggest a mafic source with alkaline mineral enrichment that evolved through magma fractionation. Despite the fact that the original geochemical characteristic of these intrusive rocks was believed to have been altered by hydrothermal fluid generated during metamorphism process and granitoid intrusions. Most of the intrusive rock samples exhibit calc-alkaline features (Fig. 13b). Majority of granitic intrusions in Ethiopia intruding into the ANS are characterized by calc-alkaline composition (Ayalew and Peccerillo, 1998; Asrat *et al.*, 2001; Bullock and Morgan, 2015). This is also in line with the abundance of calc-alkaline, S-type granites intrusions in syn-collisional and/or subduction-related environments reported in another parts of Ethiopia (Asrat and Barbey, 2003; Ayalew and Peccerillo, 1998). The Alumina Saturation Index (ASI) plot to the value of (Shanda, 1943) shows that most of the Megele area intrusive rocks are peraluminous, while metabasalt rocks are moderately metaluminous (Fig. 13c). The clear division of the granitoid (granite gneiss and granodiorite) as peraluminous (S-type granites) (Fig. 13c) possibly indicates magma sources generated from subduction of plates of sedimentary rock affinity at the collisional environment. According to (Frost *et al.*, 2001; Shand 1943) peraluminous granitoids (S-type granites) are produced by partial melting of subducting sedimentary blocks in syn-collisional complexes. The silica-rich, mica-bearing granodiorite of the Megele area, which is enriched by albite and calcium aluminum-rich minerals, with few mafic minerals, could represent proof of molten magma generated at syn-COLG and/or subduction setting (Asrat and Barbey, 2003; Ayalew and Peccerillo, 1998).

### 5.3 Tectonic setting implication

The geochemistry of granitoid and basaltoids has been used as a proxy of tectonic evolution (Pearce *et al.*, 1984; Rollinson, 1993). The tectonic discrimination diagrams generated by using incompatible trace element variation (Pearce *et al.*, 1984; Fig. 16 and Pearce, 1982; Fig. 15) support classification based on major element and assist in inferring types and source of magma, processes, and tectonic environment. Several investigations have revealed that intrusive rocks disclose complicated routes linking tectonic processes to geochemical fingerprints, such as trace element mobility during

deformation and hydrothermal changes. Scholars like (Pearce *et al.*, 1984; Goldfarb *et al.*, 2001; Saunders *et al.*, 2014) have demonstrated that immobile trace elements (such as Rb, Y, and Nb) can be used to characterize the diverse tectonic setting of magmatic rocks. Pearce *et al.*, (1984) used the combinations of these trace elements (like Rb, Y, and Nb) to discriminate the tectonic setting of magmatic rocks due to their relative stability during alteration and metamorphic processes.

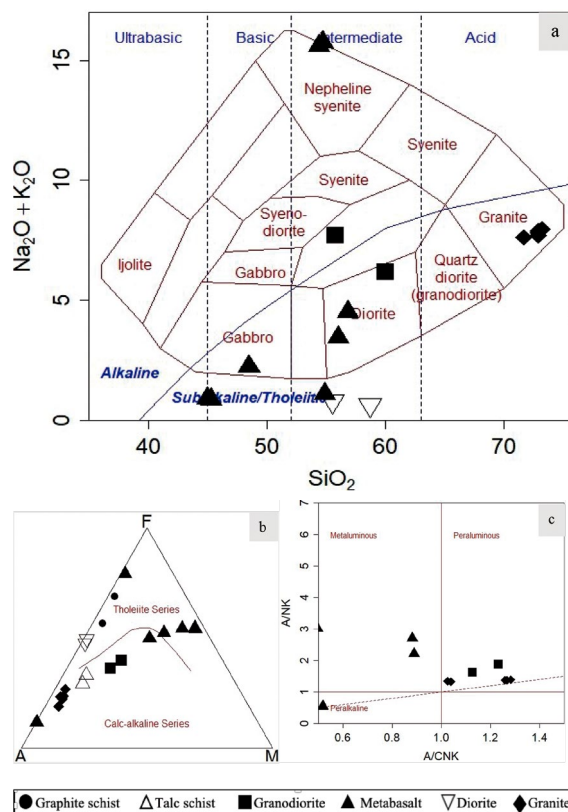


**Figure 13.** Classification diagrams of; (a) TAS classification (after Cox *et al.*, 1979) (TA: total alkalis, S: silica); (b) The AFM classification; (after Irvine and Barager, 1971) (A: total alkalis, F: total Iron, and M: MgO); and (c) the ASI classification A/NK vs. A/CNK (A =  $\text{Al}_2\text{O}_3$ , N =  $\text{Na}_2\text{O}$ , K =  $\text{K}_2\text{O}$ , C =  $\text{CaO}$ ) (after Shanda, 1943).

Pearce (1982) revealed that the Ti-Zr diagram could be used to characterize basalts of Island-arc tholeiitic, calc-alkaline, and MORB affinity. Thus, the combination of Rb-(Y+Nb) and Nb-Y cross plot have been used to discriminate the tectonic setting of the Neoproterozoic intrusive rocks from the Megele area that have only been metamorphosed to amphibolite facies. As a result, the Neoproterozoic granitoid rocks from the Megele area plotted on the volcanic arc granite (VAG) and VAG + Syn-COLG fields of the Rb-(Y + Nb) and Nb-Y cross plots, respectively (Fig. 14 a and b), showing that these granitoids are generated in subduction plate boundaries. On the other hand, the Megele area metabasalt which is metaluminous to slightly peraluminous, sub alkaline tholeiitic basalts (Fig. 13a, b respectively) plot on the MORB field of the Zr-Ti diagram (Fig. 15). The nature of these rocks (i.e., calc-alkaline, peraluminous character, as well as the weak metaluminous) are in agreement with the tectonic environment of most granitoid intrusions within a volcanic arc granite (VAG) and perhaps syn-COLG zone (Asrat, Barbey and Gleizes, 2001). Most of the peraluminous intrusions are formed from magma generated from mantle at volcanic arc granites (VAG) setting. The partial melting of basaltic magma generated at subduction setting could also generated peraluminous intrusions (Harris, Pearce and Tindle, 1986). The syn-collisional (syn-COLG) granitoids are thought to be produced at orogenic belts, with relatively high Rb/Zr and Ta/Nb ratios and low K/Rb ratios, while basaltic magmas are characterized by enrichment of selective LILE (Harris *et al.*, 1986). Other scholars (e.g., Taylor and McLennan, 1995) revealed that the enrichment in trace elements like Th and

U, as well as depletion in Ba, Nb, Sr, P, and Ti (Fig. 15b, d respectively), are common in magma generated related to arc environment. On the other hand, metamorphic alteration in the Megele area Neoproterozoic intrusive rocks may have caused migration of large ion lithophile elements (LILE) potentially overwriting the initial geochemical signature (Rollinson, 1993). For example, Rb enrichment in granite gneiss is mostly associated with growth of mica (biotite and muscovite) following potassic alteration. The depletion in Rb in the granodiorite and diorite rocks of Megele area, on the other hand, could be linked to chloritization caused by sericitic alteration of feldspar by hydrolysis process in the presence of K, S, and OH (Pearce *et al.*, 1984). The increase in concentration of LILE compared to HFSE (Fig. 16a and b, respectively) in the intrusive rocks of Megele area suggests subduction setting, implying that they were formed by calc-alkaline magmas containing considerable inputs from assimilation of disintegrated felsic crust.

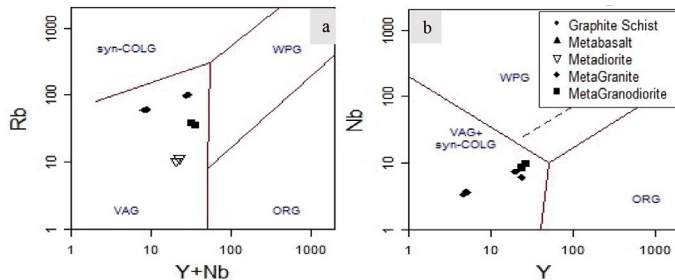


**Figure 14.** Tectonic setting discrimination of intrusive rocks from the Megele area showing: (a) all the granitoids plotted in VAG on the Rb - (Y + Nb) cross plot and (b) all the granitoids plotted in VAG+syn-COLG on the Nb-Y diagrams (after Pearce *et al.*, 1984). Note: VAG stands for volcanic arc granites; ORG stands for oceanic ridge granites; WPG stands for within plate granites; Syn-COLG stands for syn-collision granites.

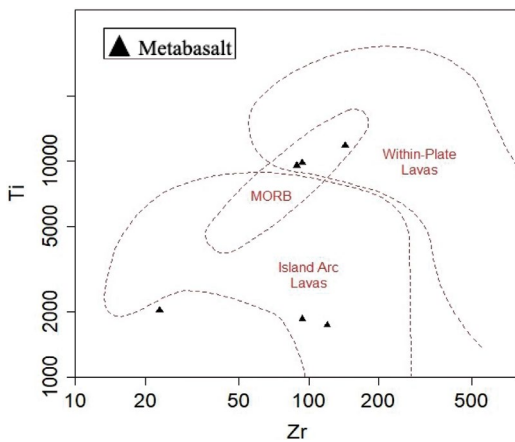


**Figure 15.** Tectonic setting discrimination of the Megele area metabasalt using Zr vs. Ti cross plot (after Pearce, 1982).

### 5.4 REE pattern

The Megele region granitoid and metabasalt rocks show a slight enrichment in LREE relative to HREE on a chondrite REE plot normalized to the value of (Nakamura, 1974) as shown on fig 14 a, b, c and d respectively. In comparison to HREE of intrusives and metabasalt, the REE pattern (Fig. 16) shows a significant enrichment in LREE. This is in agreement with the general REE pattern of VAG of the other areas (e.g., Ujuga granitoid of Western Ethiopia) (Kebede *et al.*, 1999). This is probably due to the basaltic magma enriched in LREE, that could be generated from subducted sediment slabs at a subduction zone (e.g., Warkisa *et al.*, 2021 and references therein). The fluctuation in the concentration of major oxides and trace elements with

increasing SiO<sub>2</sub> concentration (Fig. 12) indicates that granitoid rocks of the Megele area experienced fractional crystallization. The primitive mantle normalized REE diagram for both granitoid and metabasalt shows decrease in the concentration of some trace elements like Ba, Nb, Sr, P, and Ti (Fig. 16c, d), suggests that these elements are present in the fractionated magma. The segregation of plagioclase and k-feldspar minerals from the evolving magmatic fluid could be responsible for the observed negative Eu anomaly and depletion in the concentration of Ba and Sr (Rollinson, 1993; Fig. 16a, b). The depletion of Nb-Ti could have been caused by the segregation of Titanium bearing mineral phases like rutile, titanite and ilmenite from evolving melt (Ngatcha *et al.*, 2019 and reference there in). While the weak troughs in P reflected the segregation of accessory minerals apatite from the melt. Some researchers (Chappel *et al.*, 2012) argued that it could be challenging to produce considerable volumes of magma of peraluminous composition by removing ferromagnesian minerals. Therefore, the peraluminous feature of granite gneisses was most likely caused by the melting process (Ngatcha *et al.*, 2019). The Megele area Neoproterozoic granitoids show deep to moderately negative Eu anomaly that might be related to fractionating plagioclase (Rollinson, 1993). The proportionally higher concentration of LREE compared to HREE and negative Eu anomaly (Eu/Eu\* = 0.60–0.95, except for one (ATP-G5 where Eu/Eu\* = 1.02)) in addition to lower concentrations of Ca and Sr, indicates fractionation of plagioclase (Rollinson, 1993). The hydrothermal alteration is indicated by enrichment of Eu anomaly particularly in one of the granite gneiss sample (ATP-G5 where Eu/Eu\* = 1.02) probably due to chemical contribution from hydrothermal fluid (Dawood *et al.*, 2005). The trace element enrichment in both granitoid (Fig. 16c) and metabasalt (Fig. 15d) is coherent to magma derived from reworked crustal impute (Clements and Stevens, 2012).

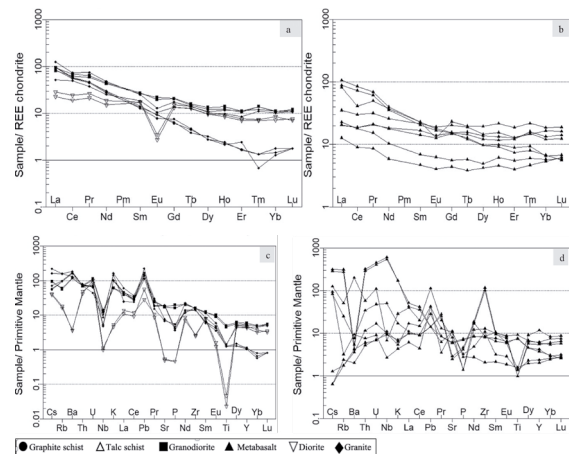


**Figure 16.** Diagram showing: (a, b) trace and RE element of Megele area intrusive rocks vs. chondrite, normalizing values are from (Nakamura 1974), and (c, d) trace element of Megele area intrusive rocks vs. primitive mantle, normalizing values are from (Sun and McDonough, 1989).

### Conclusions

The major conclusions of this study are:

- The study area (Megele) in the Sirkole Domain is comprised of Neoproterozoic granite gneiss, granodiorite, diorite, amphibole schist, quartz-graphite schist, and metabasalt rocks which has been metamorphosed from lower green-schist facies to lower amphibolite facies as indicated by mineral assemblages such as albite + muscovite + chlorite + prehnite + epidote + quartz and actinolite + hornblende + epidote + garnet respectively.
- The Neoproterozoic granitoid geochemical signatures of Megele area indicates dominantly calc-alkaline, peraluminous to slightly metaluminous, S-type granites produced by fractionation of basaltic magma that has been generated from mantle through subduction of sediment laden crustal slabs at subduction environment.

- The REE chondrite and primitive mantle-normalized trace element patterns reveal enrichment in LREE compared to HREE, as well as enrichment in Th, U, Sn, and Mo, with depletion in Ba, Nb, Sr, P, Eu, and Ti and negative Eu anomaly. This indicates fractionation of underplating LREE-enriched magma from reworked basaltic slab underlain by sediments at subduction zone.

### Acknowledgement

This research is part of the Ph.D. dissertation work of (T.O.), which was supported by the African Union through the Pan African University Institute of Life and Earth Sciences (including health and agriculture), PAULESI. The comments and criticism of the editor(s) and reviewer(s) to the improvement of this paper are greatly appreciated.

### Reference:

- Abdelsalam, M. G., & Stern, R. J. (1996). Sutures and Shear Zones in the Arabian-Nubian Shield. *African Journal of Earth Science*, 22 (3), 289-310. DOI:10.1016/S0899-5362(97)00003-1
- Alemu, T., & Abebe T. (2007). Geology and Tectonic Evolution of the Pan African Tulu Dimtu Belt, Western Ethiopia. *Online Journal of Earth Sciences* 1(1), 24-42.
- Allistair, A., & Tadesse G. (2003). Geological Setting and Tectonic Subdivision of the Neoproterozoic Orogenic Belt of Tulu Dimtu, Western Ethiopia. *Journal of African Earth Sciences*, 36, 329-343. DOI.org/10.1016/S0899-5362(03)00045-9
- ALS (2021). Analytical Testing Services Manual. <https://www.alsglobal.com/>.
- Asrat, A., Barbey, P., & Gleizes, G. (2001). The Precambrian Geology of Ethiopia: A Review. *Africa Geoscience Review*, 8, 271-288.
- Asrat, A., & Barbey, P. (2003). Petrology, Geochronology and Sr-Nd Isotopic Geochemistry of the Konso Pluton, South-Western Ethiopia: Implications for Transition from Convergence to Extension in the Mozambique Belt. *International Journal of Earth Sciences*, 92(6), 873-890. DOI.org/10.1007/s00531-003-0360-9
- Assefa, G., Di Paola G. M., & Valera, R. (1981). Plate Tectonics and Metallogenic Processes in Ethiopia (Preliminary Report). *Rendiconti della Societa Italiana di Mineralogia e Petrologia*, 37(2), 861-867.
- Ayalew, T. (1997). Metamorphic and Structural Evolution of the Gore-Gambella Area, Western Ethiopia. *SINET: Ethiopian Journal of Science*, 20(2). DOI: 10.4314/sinet.v20i2.18103.
- Ayalew, T., Bell, K., Moore, J.M., & Parrish, R. R. (1990). U-Pb and Rb-Sr Geochronology of the Western Ethiopian Shield. *Geological Society of America Bulletin*, 102(9), 1309-1316.
- Ayalew, T., & Johnson, T. E. (2002). The Geotectonic Evolution of the Western Ethiopian Shield. *SINET: Ethiopian Journal of Science*, 25(2), 227-252. DOI:10.4314/sinet.v25i2.18082.
- Ayalew, T., & Peccerillo, A. (1998). Petrology and Geochemistry of the Gore-Gambella Plutonic Rocks: Implications for Magma Genesis and the Tectonic Setting of the Pan-African Orogenic Belt of Western Ethiopia. *Journal of African Earth Sciences*, 27(3-4), 397-416. DOI.org/10.1016/S0899-5362(98)00070-0
- Bingen, B., Jacobs, J., Viola, G., Henderson, I. H. C., Skår, O., Boyd, R., Thomas, R. J., Solli, A., Key, M., & Daudi, E. X. F. (2009). Geochronology of the Precambrian Crust in the Mozambique Belt in NE Mozambique, and Implications for Gondwana Assembly. *Precambrian Research*, 170(3-4), 231-255. DOI.org/10.1016/j.precamres.2009.01.005
- Blades, M. L., Collins, A. S., Justin, J. F., Payne, L., Xu, X., Alemu, T., Woldetinsae, G., Richard, C. C., & Taylor, J. M. (2015). Age and Hafnium Isotopic Evolution of the Didesa and Kemashi Domains, Western Ethiopia. *Precambrian Research*, 270, 267-84. DOI.org/10.1016/j.precamres.
- Blades, M. L., Collins, A. S., Justin, J. F., Alemu, T., & Woldetinsae, G. (2019). The Origin of the Ultramafic Rocks of the Tulu Dimtu Belt, Western Ethiopia-Do They Represent Remnants of the Mozambique Ocean? *Geological Magazine*, 156(1), 62-82. DOI.org/10.1017/S0016756817000802.
- Bullock, L. A., & Morgan, O. J. (2015). A New Occurrence of (Gold-Bearing) Graphite in the Assosa Region, Benishangul-Gumuz State, Western Ethiopia. *International Journal of Earth Sciences and Engineering*, 5. DOI: 10.17265/2159-581X/2015.07.003
- Bullock, L. A., & Morgan, O. J. (2018). The Asosa Region of Western Ethiopia: A Golden Exploration Opportunity. *The Geologists' Association & The Geological Society of London, Geology Today*, 34(1). DOI.org/10.1111/gto.12217
- Chappell, B. W., Bryant, C. J., & Wyborn, D. (2012). Peraluminous I-Type Granites. *Lithos*, 153, 142-153. DOI.org/10.1016/j.lithos.2012.07.008.
- Clemens, J. D., Stevens, G. (2012). What Controls Chemical Variation in Granitic Magmas? *Lithos*, 134-135: 317-329. DOI.org/10.1016/j.lithos.2012.01.001.
- Collins, A. S. (2006). Madagascar and the Amalgamation of Central Gondwana. *Gondwana Research*, 9(1-2), 3-16. DOI.org/10.1016/j.gr.2005.10.001
- Cox, K. G., Bell, J. D., & Pankhurst, R. J. (1979). *Trace Elements in Igneous Processes*. In: Cox, K. G., Bell, J. D., & Pankhurst, R. J. (Eds.). *The Interpretation of Igneous Rocks*, Springer, Dordrecht, 332-359. DOI.org/10.1007/978-94-017-3373-1\_14.
- Dawood, Y. H., Saleh, G. M., & Abd El-Naby, H. H. (2005). Effects of Hydrothermal Alteration on Geochemical Characteristics of the El Sukkari Granite, Central Eastern Desert, Egypt. *International Geology Review*, 47(12), 1316-1329. DOI.org/10.2747/0020-6814.47.12.1316.
- Fritz, H., Abdelsalam, M., Ali, K. A., Bingen, B., Collins, A. S., Fowler, A. R., Ghebreab, W., Hauenberger, C. A., Johnson, P. R., Kusky, T. M., Macey, P., Muhongo, S., Stern, R. J., & Viola, G. (2013). Orogen Styles in the East African Orogen: A Review of the Neoproterozoic to Cambrian Tectonic Evolution. *Journal of African Earth Sciences*, 86, 65-106. DOI.org/10.1016/j.jafrearsci.2013.06.004.
- Fritz, H., Tenczer, V., Hauenberger, C. A., Wallbrecher, E., & Hoinkes, G. (2005). Central Tanzanian Tectonic Map: A Step Forward to Decipher Proterozoic Structural Events in the East African Orogen. *Tectonics*, 24(6). DOI.org/10.1029/2005TC001796
- Frost, B. R., Barnes, C. G., Collins, W. J., Arculus, R. J., Elles, D. J., & Frost, C. D. (2001). A Geochemical Classification for Granitic Rocks. *Journal of Petrology*, 42(11), 2033-2048. DOI: 10.1093/petrology/42.11.2033
- Goldfarb, R. J., Groves, D. I., & Gardoll, S. (2001). Orogenic Gold and Geologic Time: A Global Synthesis. *Ore Geology Reviews*, 18(1-2), 1-75. DOI.org/10.1016/S0169-1368(01)00016-6.
- Harris, N. B. W., Pearce, J. A., & Tindle, A. G. (1986). Geochemical Characteristics of Collision-Zone Magmatism. *Geological Society Special Publication*, 19, 67-81. DOI: 10.1144/GSL.SP.1986.019.01.04
- Johnson, P. R., Andresen, A., Collins, A. S., Fowler, A. R., Fritz, H., Ghebreab, W., Kusky, T., & Stern, R. J. (2011). Late Cryogenian-Ediacaran History of the Arabian-Nubian Shield: A Review of Depositional, Plutonic, Structural, and Tectonic Events in the Closing Stages of the Northern East African Orogen. *Journal of African Earth Sciences*, 61(3), 167-232. DOI.org/10.1016/j.jafrearsci.2011.07.003.
- Johnson, P., & Woldehaimanot, B. (2003). Development of the Arabian-Nubian Shield: Perspectives on Accretion and Deformation in the Northern East African Orogen and the Assembly of Gondwana. *Geological Society Special Publication*, 206, 289-325. DOI: 10.1144/GSL.SP.2003.206.01.15
- Kazmin, V. (1971). Precambrian of Ethiopia. *Nature Physical Science*, 230. <https://www.nature.com/articles/physci230176a0#citeas>.
- Kazmin, V., Shifferaw, A., & Balcha, T. (1978). The Ethiopian Basement: Stratigraphy and Possible Manner of Evolution. *Geologische Rundschau*, 67(2), 531-546. DOI.org/10.1007/BF01802803.

- Kebede, T., Koeberl, C., & Koller, F. (1999). Geology, Geochemistry and Petrogenesis of Intrusive Rocks of the Wallagga Area, Western Ethiopia. *Journal of African Earth Sciences*, 29(4), 715–734. DOI.org/10.1016/S0899-5362(99)00126-8.
- Nakamura, N. (1974). Determination of REE, Ba, Fe, Mg, Na and K in Carbonaceous and Ordinary Chondrites. *Geochimica et Cosmochimica Acta*, 38(5), 757–775. DOI.org/10.1016/0016-7037(74)90149-5
- Ngatcha, R. L., Okunlola, O. A., Suh, C. E., Ateh, K. I., & Hofmann, A. (2019). Petrochemical Characterization of Neoproterozoic Colomine Granitoids, SE Cameroon: Implications for Gold Mineralization. *Lithos*, 344–345, 175–192. DOI.org/10.1016/j.lithos.2019.06.028.
- Pearce, J. A. (1982). *Trace Element Characteristics of Lavas from Destructive Plate Boundaries*. In: Thorpe R.S. (Ed.). *Andesites: Orogenic Andesites and Related Rocks*. John Wiley and Sons, 525–548.
- Pearce, J. A., Harris, N. B. W., & Tindle, A. G. (1984). Trace Element Discrimination Diagrams for the Tectonic Interpretation of Granitic Rocks. *Journal of Petrology*, 25(4), 956–983. DOI: 10.1093/petrology/25.4.956.
- Rollinson, H. R. (1993). *Using Geochemical Data: Evaluation, Presentation, Interpretation*. Pearson Prentice Hall, 1.
- Saunders, J. A., Hofstra, A. H., Goldfarb, R. J., & Reed, M. H. (2014). *Geochemistry of Hydrothermal Gold Deposits*. 13 Treatise on Geochemistry, 2nd ed. Elsevier Ltd. DOI.org/10.1016/B978-0-08-095975-7.01117-7.
- Shand, S. J. (1943). *Eruptive Rocks*. 2nd ed. John Wiley, New York.
- Stern, R. J. (1994). Arc Assembly and Continental Collision in the Neoproterozoic East African Orogen: Implications for the Consolidation of Gondwanaland. *Annual Review of Earth & Planetary Sciences*, 22, 319–351. DOI.org/10.1146/annurev.earth.22.050194.001535.
- Stern, R. J., Johnson, P. R., Kröner, A., & Yibas, B. 2004. Neoproterozoic Ophiolites of the Arabian-Nubian Shield. *Developments in Precambrian Geology*, 13(C), 95–128. DOI.org/10.1016/S0166-2635(04)13003-X
- Sun, S. S., & McDonough, W. F. (1989). Chemical and Isotopic Systematics of Oceanic Basalts: Implications for Mantle Composition and Processes. *Geological Society Special Publication*, 42(1), 313–345. DOI: 10.1144/GSL.SP.1989.042.01.19
- Tadesse, S., Milesi, J. P., & Deschamps, Y. (2003). Geology and Mineral Potential of Ethiopia: A Note on Geology and Mineral Map of Ethiopia. *Journal of African Earth Sciences*, 36(4), 273–313. DOI.org/10.1016/S0899-5362(03)00048-4
- Taylor, S. R., & McLennan, S. M. (1995). The Geochemical Evolution of the Continental Crust. *Reviews of Geophysics*, 33(2), 241–65. DOI.org/10.1029/95RG00262
- Tulloch, A. J. (1979). Secondary Ca-Al Silicates as Low-Grade Alteration Products of Granitoid Biotite. *Contributions to Mineralogy and Petrology*, 69(2), 105–117. DOI.org/10.1007/BF00371854
- De Waele, B., Kampunzu, A. B., Mapani, B. S. E., & Tembo, F. (2006). The Mesoproterozoic Irumide Belt of Zambia. *Journal of African Earth Sciences*, 46(1–2), 36–70. DOI.org/10.1016/j.jafrearsci.2006.01.018
- Warkisa, G., Asrat, A., Omitogun, A. A., & Oljira, T. (2021). Petrogenesis of Gold-Hosting Neoproterozoic Syenite from the Tulu Kapi Area, Western Ethiopia. *Journal of African Earth Sciences*, 176. DOI: 10.1016/j.jafrearsci.2021.104145
- Wolde, B., Desta, Z. A., & Gonzalez, J. J. (1996). Neoproterozoic Zirconium-Depleted Boninite and Tholeiitic Series Rocks from Adola, Southern Ethiopia. *Precambrian Research*, 80, 261–279. DOI.org/10.1016/S0301-9268(96)00018-6

